Transcranial electrical stimulation generates electric fields in deep human brain structures

Samuel Louviot, Louise Tyvaert, Louis G. Maillard, Sophie Colnat-Coulbois, Jacek Dmochowski, Laurent Koessler

Brain Stimulation 15 (2022) 1–12

Contents lists available at ScienceDirect

Brain Stimulation

journal homepage: http://www.journals.elsevier.com/brain-stimulation

Transcranial Electrical Stimulation generates electric fields in deep human brain structures

Samuel Louviot [a], Louise Tyvaert [a, b], Louis G. Maillard [a, b], Sophie Colnat-Coulbois [a, c], Jacek Dmochowski [d], Laurent Koessler [a, *]

[a] Université de Lorraine, CNRS, CRAN, F-54000, Nancy, France
[b] Université de Lorraine, CHRU-Nancy, Service de Neurologie, F-54000, Nancy, France
[c] Université de Lorraine, CHRU-Nancy, Service de Neurochirurgie, F-54000, Nancy, France
[d] Department of Biomedical Engineering, City College of New York, New York, NY, USA

ARTICLE INFO

Article history:
Received 5 March 2021
Received in revised form
21 October 2021
Accepted 1 November 2021
Available online 4 November 2021

Keywords:
Transcranial electrical stimulation
Human *in-vivo*
Stereoelectroencephalography
Electric field
HD electrodes
Hippocampus

ABSTRACT

Background: Transcranial electrical stimulation (TES) efficiency is related to the electric field (EF) magnitude delivered on the target. Very few studies (n = 4) have estimated the *in-vivo* intracerebral electric fields in humans. They have relied mainly on electrocorticographic recordings, which require a craniotomy impacting EF distribution, and did not investigate deep brain structures.
Objective: To measure the electric field in deep brain structures during TES in humans *in-vivo*. Additionally, to investigate the effects of TES frequencies, intensities, and montages on the intracerebral EF.
Methods: Simultaneous bipolar transcranial alternating current stimulation and intracerebral recordings (SEEG) were performed in 8 drug-resistant epileptic patients. TES was applied using small high-definition (HD) electrodes. Seven frequencies, two intensities and 15 montages were applied on one, six and one patients, respectively.
Results: At 1 mA intensity, we found mean EF magnitudes of 0.21, 0.17 and 0.07 $V \cdot m^{-1}$ in the amygdala, hippocampus, and cingulate gyrus, respectively. An average of 0.14 ± 0.07 $V \cdot m^{-1}$ was measured in these deep brain structures. Mean EF magnitudes in these structures at 1Hz were 11% higher than at 300Hz ($+0.03$ $V \cdot m^{-1}$). The EF was correlated with the TES intensities. The TES montages that yielded the maximum EF in the amygdalae were T7-T8 and in the cingulate gyri were C3-FT10 and T7-C4.
Conclusion: TES at low intensities and with small HD electrodes can generate an EF in deep brain structures, irrespective of stimulation frequency. EF magnitude is correlated to the stimulation intensity and depends upon the stimulation montage.

1. Introduction

Transcranial Electrical Stimulation (TES) is one of the most developed non-invasive brain stimulation technique. Both transcranial direct current stimulation (tDCS) [1] and transcranial alternating current stimulation (tACS) [2] have shown promise to understand brain function [3] and as an investigational treatment for neurological [4,5] and psychiatric [6,7] disorders. At the neuronal scale (*in-vitro* experiments), the mechanism underlying the beneficial effects of TES relates to the modulation of the neuronal membrane potential by the electric field (EF) applied, and potentially the plastic changes that may ensue [2,8–16]. Under the ideal conditions of *in-vitro* experiments, an EF as low as 0.2–0.5 $V \cdot m^{-1}$ can shift spike timing [11,14,17–19]. Our understanding of the EF generated in the brain when delivering low-frequency electric currents with scalp electrodes has been derived from computational models of the current flow [20–22]. The type of electrodes, their montages and the current intensities applied, which are crucial to generate a sufficient EF to modulate the neuronal population, are still a matter of debate [23–26]. One of the biggest challenges in TES is generating an EF in deep brain structures such as the limbic system [27,28] that would have a truly significant impact at the clinical level (e.g., improvement of Epilepsy or Alzheimer's diseases conditions) and at the fundamental level (e.g., understanding of memory processes, including learning).

* Corresponding author.
E-mail address: laurent.koessler@univ-lorraine.fr (L. Koessler).

https://doi.org/10.1016/j.brs.2021.11.001

TES effects in deep brain structures have generated two major issues in the scientific community.

The first issue concerns the mechanisms underlying the beneficial effects of TES in deep brain structures. In-vivo non-human primate studies have found spike timing changes induced by tACS in the hippocampus and basal ganglia and measured EF (peak field strengths of 0.3 $V \cdot m^{-1}$) in these structures [29,30]. Clinical studies have also shown [31–33] encouraging results in mesial temporal lobe epilepsy (i.e., decrease of seizure and interictal discharge frequencies). However, currently, the ability to directly neuromodulate (i.e., without other indirect activations) deep brain structures is under considerable debate, especially since several studies in humans and non-human animal models suggest alternative peripheral mechanisms [34–37].

The second issue concerns the ability of electric currents to penetrate tissues to reach deep brain regions at low TES intensities (safety issue). Several TES studies did not induce volume conduction and little to no EF magnitudes within the brain volume [38–40]. The most frequent reasons advanced for this lack of findings are the decrease of the EF due to the depth between the stimulation electrodes and the anatomical target [41], and the head tissue resistivities-especially the skull's high resistivity [42]. Yet, computational studies have found deep brain EF hotspots with realistic MRI-based modelling [27,43–45]. Moreover, other recent studies reported an electric field induced by TES using *in-vivo* human investigations [41,46–48]. Opitz et al. reported EF magnitudes up to 0.5 V m^{-1} in the superficial cortex for a 1 mA tACS using saline soaked sponge electrodes (25 cm^2) and Huang et al. presented an EF of 0.4 $V \cdot m^{-1}$ in cortical structures for a 2 mA tACS using rubber electrodes (4 cm^2). These results can be biased because they relied on combined stereoelectroencephalographic (SEEG) and electrocorticographic (ECoG) investigation in which large skull defects were performed that can affect these intracerebral EF magnitudes [49]. In a computational study, it was demonstrated that conductivity of large skull defects increased and current were concentrated in cortex underlying the defect area (Datta et al., 2010).

Using deep brain stimulation electrodes, two studies estimated the global electric fields achieved in subthalamic nuclei and internal globus pallidus using two distant electrodes (2 cm–4 cm) and a DC experiment ($n = 2$ patients; EF ranged from 0.19 to 0.26 $V \cdot m^{-1}$ at 4 mA intensity) [47] or an AC experiment [48] ($n = 1$ patient; EF_{max}: 0.08 $V \cdot m^{-1}$ for an intensity of 1 mA).

Considering these limited and variable observations, which leave the two issues mentioned above wide open, the main objective of the present study was to measure the intracerebral EF during TES with an emphasis on deep brain structures. To do so, we leveraged the unique ability to record the EF *in-vivo* in humans using depth electrodes implanted in drug-resistant epileptic patients (SEEG) by applying TES using small high-definition (HD) electrodes and low intensity ($\leq$1 mA). Our secondary objectives were, first, to investigate the influence of TES frequency, intensity, and montages on EF magnitudes and second, to investigate the influence of the depth (i.e., the distance between the depth electrodes and the TES electrodes) on EF magnitudes.

2. Materials & methods

2.1. Patients

Eight patients (4 females and 4 males; age: 30 ± 11 years old) with focal drug-resistant epilepsy were prospectively included in this study. Patients were informed early and gave their consent prior to participation (NCT03644732). Patients were instructed to report any discomfort during TES and were told that the stimulation could be stopped if they felt pain at any time. They were all candidates for presurgical evaluation. Their standard presurgical evaluation included: neuropsychological tests and long-term (5-day period) high-resolution electroencephalographic (EEG) video recordings combined with electrical source imaging analysis, positron emission tomography (PET) and high-resolution magnetic resonance imaging (MRI). SEEG was performed in these patients to complete the presurgical evaluation to better define the epileptogenic zone and the surrounding functional area [50]. In all included patients, SEEG allowed delineating a single and spatially limited epileptogenic zone.

2.2. Stereoelectroencephalography

For each patient, an individual SEEG implantation scheme was defined according to the presurgical evaluation and epileptogenic zone hypotheses.

Under general anesthesia, the intracerebral multi-contact electrodes (0.8 mm-diameter, from 5 to 18 Platinum/Iridium contacts with 2 mm length separated by 1.5 mm insulator; Dixi Medical®, Besançon, France) were implanted according to a standard stereotactic procedure [51]. The SEEG electrodes were inserted into a screw (2.45 mm-diameter) and secured with a tight seal to prevent cerebrospinal fluid leak. Immediately after the implantation, patients underwent a postoperative CT-scan. Using a co-registration of the CT-scan with the preoperative high-resolution MRI (voxel-based registration; SPM 8 toolbox for Matlab; MathWorks, Natick, Massachusetts), the anatomical positions of each electrode contact were determined, and potential surgical complications were inspected. Due to the minimally invasive procedure used for SEEG investigation, anatomical structures did not move in the intracranial volume (no CSF leakage and no brain swelling) and MR-CT co-registration can be assumed as very precise (<1 mm [52]).

In addition to the intracerebral multi-contact electrodes, 27 scalp electrodes were placed according to an adapted 10/20 system [53]. Visual review of the simultaneous EEG-SEEG recordings was done prior to the tACS experiments. Moreover, the visual review checked for unusual electrophysiological activity such as breach rhythm which is defined as a focal increase in the amplitude activity of alpha, beta and mu rhythms which tends to develop over or near the area of a bony skull defect, such as after craniotomy or cranial surgery [54]. In our study, no breach rhythm was observed.

During tACS experiments, SEEG signals were recorded with a 256-channel (2 × 128 channels) amplifier with a 10 kHz sampling rate, 16 bits resolution at 0.25 μV/bit, a high-pass filter 1st order at 0.3 Hz, an input impedance superior to 10 GΩ and an input signal range ± 8.191 mV (NeuroPort™ System by Blackrock® Microsystems, Salt Lake City, UT, USA). The recording device's ground was set on the right foot, away from the TES electrodes and the recording reference, which was set on a deep SEEG contact.

2.3. Transcranial electrical stimulation

Before the intracerebral electrode withdrawal, tACS were performed using two HD electrodes (12 mm external diameter; Soterix Medical®, New York, NY, USA). Both were inserted in an electrode-holder (24 mm diameter) filled with a conductive gel, creating a 4.52 cm^2 stimulation area on the scalp for each electrode. The impedances were checked before, during, and after each stimulation and were always inferior or equal to 5kΩ. According to the HD electrodes' geometry, current densities generated on site were 0.11 $mA \cdot cm^{-2}$ and 0.22 $mA \cdot cm^{-2}$ for 0.5 mA and 1 mA intensities, respectively. The stimulation was delivered through these

electrodes using a multichannel TES stimulator MxN-9 (Soterix Medical®, New York, NY, USA). TACS was a bipolar sinusoidal waveform which can be expressed by:

$$s(t) = I.\sin(2\pi ft)$$

where I is the stimulation intensity in milli-Ampere (mA) (i.e., the peak to baseline value of the intensity) and *f* the stimulation frequency in Hertz (Hz).

A stimulation design (Fig. 1) was defined by its frequency, intensity, and montage. A typical session had a 2-min duration (30-s ramp up, 1-min full intensity, 30-s ramp down) at a given intensity and frequency. Each session was separated by a 1-min resting state, tACS off. During all sessions, patients were in a resting state with eyes open. For data analysis, the most superficial SEEG contacts (outside of the brain) were discarded to avoid aberrant values.

For one patient (Patient #0), tACS experiment was done using seven different frequencies (1 Hz; 3 Hz; 7 Hz; 35 Hz; 71 Hz; 140 Hz and 300 Hz). For the other patients (Patient #1–7), tACS was applied at 300 Hz only. This frequency of interest was between the large-amplitude LFP oscillations and the spiking activity i.e., in a frequency band with low neuro-electrophysiological activity. For a detailed analysis regarding the reliability of our stimulation and acquisition systems at the frequency used, see Supplementary Material (Supplementary data 1, Figs. 1–2). Finally, the TES electrode coordinates were numerically collected by fitting in Brainstorm [55] a Colin27 generic 10-10 EEG cap on the individual patient's head model.

2.4. Intracerebral electric field

This study included all eight patients. They had an average of 14 (±3) SEEG electrodes and 170 (±35) intracerebral contacts. TACS montages were defined using the MRI-CT co-registrations which showed the positions and trajectories of each intracerebral multi-contact electrode [51] and thus allowed cranio-anatomical correlations [56]. To guarantee asepsis conditions, a minimum distance of at least 5 cm was maintained between the closest implanted SEEG electrodes and the TES electrodes. To target both the hippocampus/amygdala complex and the cingulate gyri, an FT9-FT10 or T7-C4 or C3-FT10 montage was chosen. These montages were chosen to (1) get the EF's largest component along the SEEG electrodes' direction, (2) reach the deep targeted structures and (3) place as far as possible the two stimulation electrodes to maximize the current flowing inside the brain (minimizing the scalp shunt) [57,58].

Bipolar alternative current stimulations were done at two different intensities: 0.5 mA and 1 mA. The first objective was to investigate the intracerebral electric field specifically in deep brain structures such as the hippocampus, amygdala, and cingulate gyrus.

In theory, the EF is the electric potential gradient in the three directions of space (*x,y,z*):

$$\vec{E} = -\overrightarrow{grad}\,\vec{V} = -\left(\frac{\partial V}{\partial x}\overrightarrow{u_x} + \frac{\partial V}{\partial y}\overrightarrow{u_y} + \frac{\partial V}{\partial z}\overrightarrow{u_z}\right) \quad (1)$$

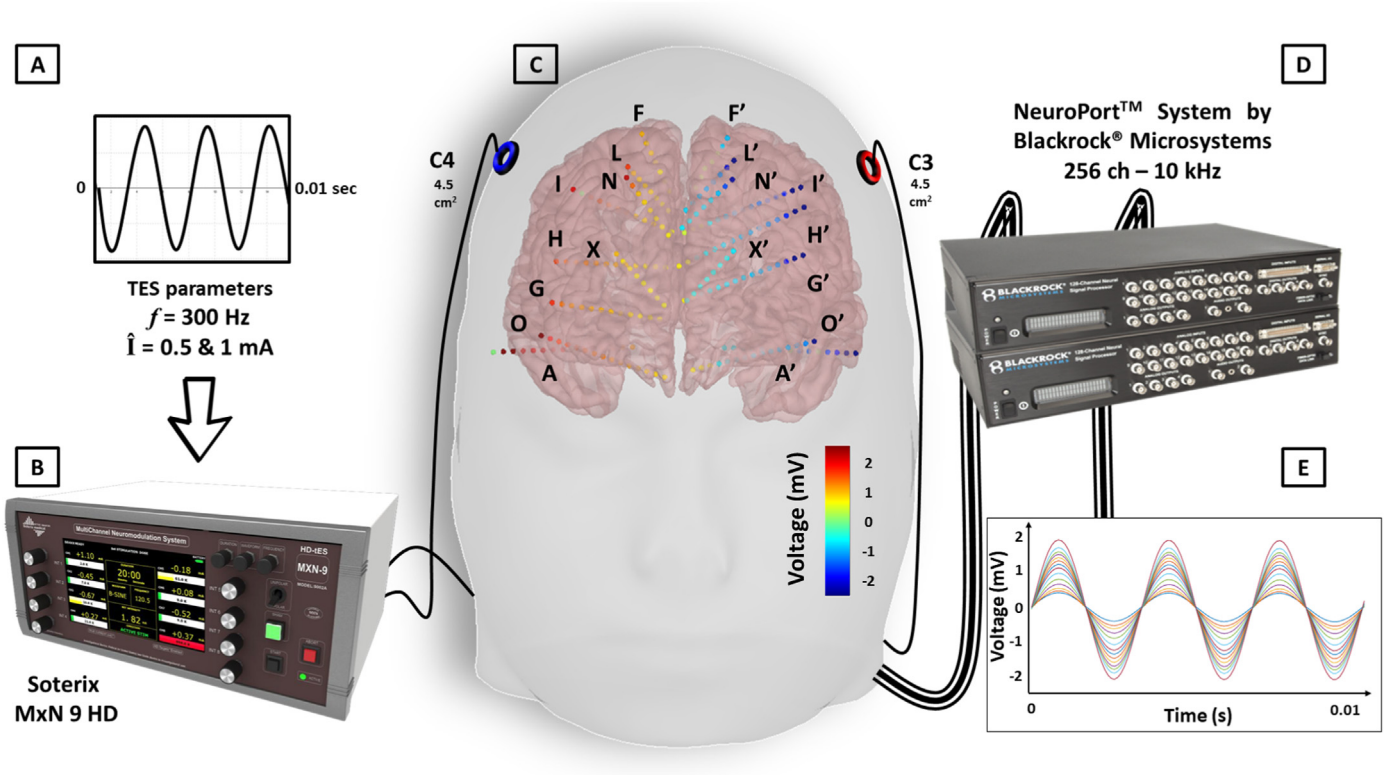

Fig. 1. Title: Simultaneous combination of transcranial alternative current stimulations (tACS) and SEEG recordings.
Caption: Bipolar sinusoidal signals at 300 Hz (part A) were delivered using a Soterix MxN stimulator (part B), and two HD ring electrodes (4.5 cm^2, active electrode in red, neutral electrode in blue) (Part C). A 256-channel amplifier (NeuroPort™ System by Blackrock® Microsystems, Salt Lake City, UT, USA) (part D) was used to record the sinusoidal signals in all intracerebral multi-contact electrodes (superimposed SEEG signals are represented in colored lines) (part E). In part C, colors represent the *in-vivo* measured voltage in all intracerebral contacts (n = 140; colored dots) using a realistic head model (patient 7) with a C3–C4 stimulation at 300 Hz and 1 mA intensity. (For interpretation of the references to color in this figure legend, the reader is referred to the Web version of this article.)

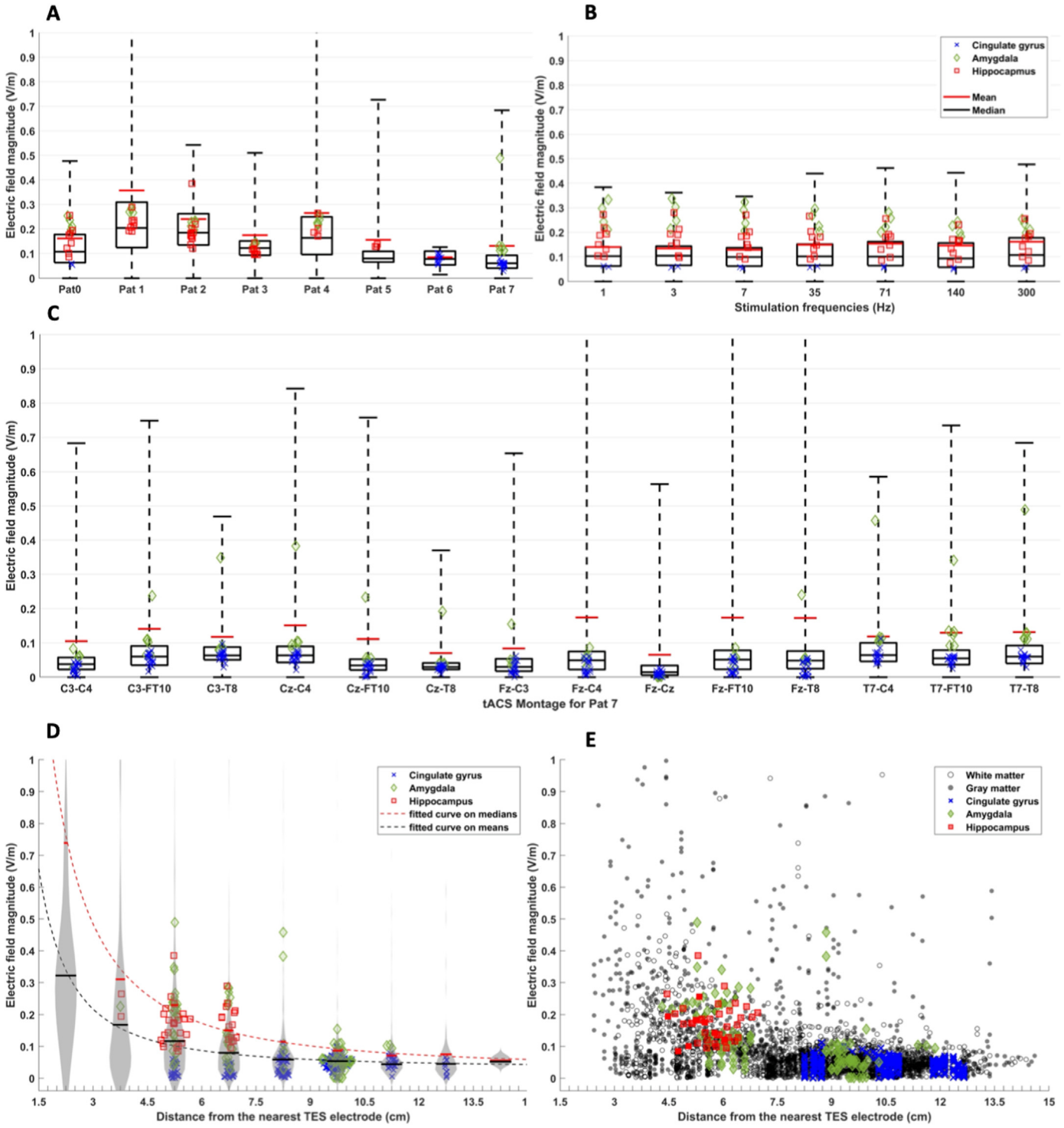

Fig. 2. Title: Electric field magnitude distribution in the cohort according to different tACS frequencies, montages, and the distance from the nearest TES electrode.
For all figures, the EF magnitudes in deep cortical structures are displayed with symbols (hippocampus: red squares, amygdala: green diamonds, cingulate gyrus: blue crosses). **A:** Electric field magnitude in the entire brain for all patients for a tACS at 300Hz and 1 mA. **B:** Electric field magnitude in the entire brain for every frequency tested in Pat 0 at 1 mA. **C:** Electric field magnitude in the entire brain for all montages tested in Pat 7 at 300Hz and 1 mA. For A, B and C: whiskers, considered as minimum and maximum values, represent 2.5 the standard-deviation of every EF magnitude distribution and boxes represent the 25th and 75th percentiles values of EF magnitudes. Black lines inside the box are the median values of the EF magnitude distribution and red lines indicate the means. **D:** Density of the EF magnitude distribution against the distance from the nearest TES electrode. Dashed lines represent the fitted power-curves from a non-linear regression on means values (in red; $R^2 = 0.99$) and median values (in black; $R^2 = 0.99$). **E:** Scattered representation of EF magnitudes against the distance from the nearest TES electrode. Gray and white dots are EF in the gray and white matter, respectively. (For interpretation of the references to color in this figure legend, the reader is referred to the Web version of this article.)

The EF along the direction x is expressed:

$$\overrightarrow{E}(x) = -\frac{dV}{dx}\overrightarrow{u_x} \quad 2$$

with $\overrightarrow{u_x}$ the unit vector along the direction x and the EF magnitude:

$$\left|\overrightarrow{E}_x\right| = -\frac{dV}{dx} \quad 3$$

Also, using $\overrightarrow{u_p}$ the unit vector, which has its module and its directionality given by 2 contiguous SEEG contacts on the same electrode, we can express the electric field along that SEEG electrode by

$$\overrightarrow{E}(p) = -\frac{dV}{dp}\overrightarrow{u_p} \quad 4$$

With dp the distance between the 2 contiguous contacts.

Thus, the EF was obtained by calculating the gradient of the voltage measured on each contact of a same SEEG electrode.

First, a baseline correction was performed. It was executed by performing a manual selection of the analysis window of the SEEG signal under stimulation, while avoiding potential DC offset and artifacts (see supplementary data 1, Fig. 3A). To do so, the raw SEEG signal was subtracted by the mean of the signal calculated in a 2-s window right before the stimulation, when patients were in a resting state (see supplementary data 1, Figs. 3 and 4).

Every baseline correction window of raw SEEG signals was visually checked, and no artifact observed.

Second, all SEEG signals were superimposed upon each other to facilitate the selection of the time window analysis (after the ramp up and before the ramp down of the tACS).

Third, a Fast Fourier Transform was computed on the SEEG signal in each contact using Matlab `fft()` function [59]. The two-sided power spectrum of the FFT was converted to a single-sided power spectrum. Then, the amplitude spectrum was obtained by calculating the square root of this single-sided power spectrum's absolute value (Bessel-Parseval theorem). Finally, to obtain our voltage values (V), the maximum value (peak) was searched in the amplitude spectrum between 297 Hz and 303 Hz with a frequency resolution of 0.016 Hz. The baseline correction (0 Hz) did not influence the voltage amplitude V at these high frequencies.

The Matlab (The MathWorks®) gradient function was used for calculating the gradient of V along a multi-contact SEEG electrode to get the EF module. This calculation was repeated for all SEEG electrodes.

For each patient and all SEEG electrodes, the mean electric field and its standard deviation were calculated (Table 1). The mean EF values for the entire brain were calculated by:

$$\overline{|E|} = \frac{1}{n}\sum_{j=1}^{n}|E|_j \quad 5$$

where n is the number of SEEG contacts and $|E|_j$ the EF magnitude calculated on a contact j.

EF distributions according to all patients, the TES frequencies and montages were displayed using boxplots with boxes represented the 25th and the 75th percentiles and whiskers showed the EF magnitude values spread with a coverage of 2.5 the standard deviation.

The position of each intracerebral contact was automatically detected in the individual CT-scan [60] and visually defined using patients' MRI-CT co-registration. Automatic segmentation method (CAT12, SPM12 toolbox; [61]) allowed to identify gray and white matters.

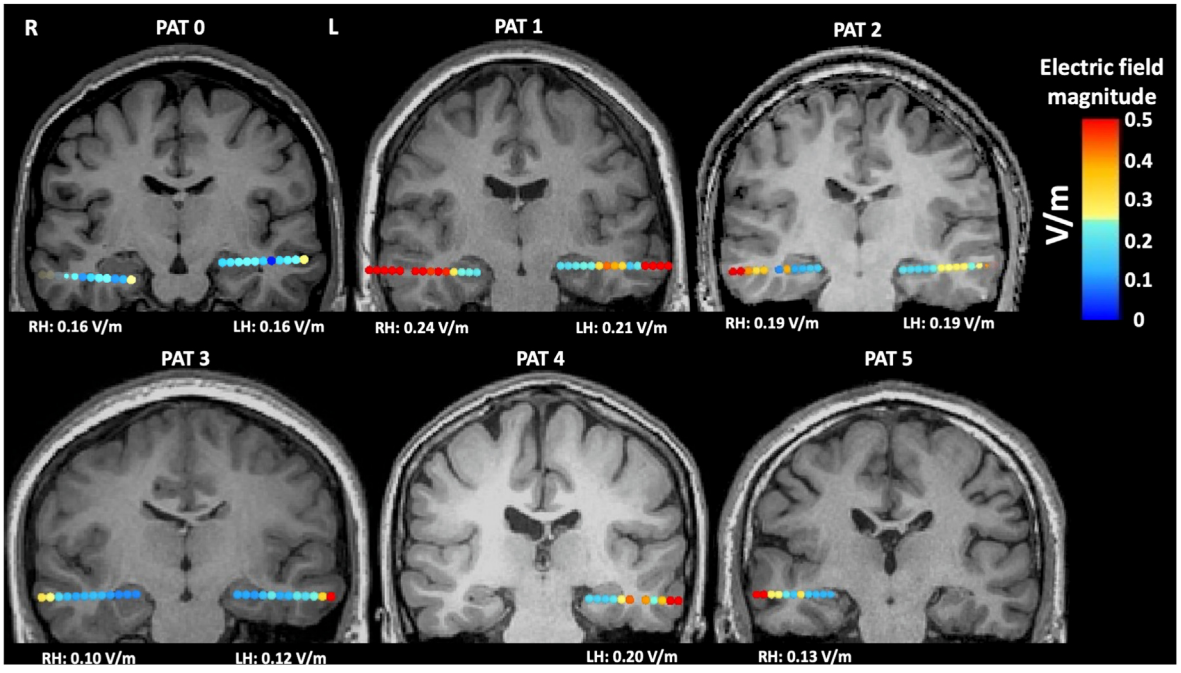

Fig. 3. Title: Empirical electric fields (EF) in the hippocampi.
Caption: Empirical electric fields (EF) in the hippocampi for a 1 mA tACS using FT9-FT10 montage. Below each individual MRI with the reconstructed SEEG electrodes, the mean EF values of SEEG contacts within the deep structures was indicated. (L: left, R: right, H: Hippocampus). (For interpretation of the references to color in this figure legend, the reader is referred to the Web version of this article.)

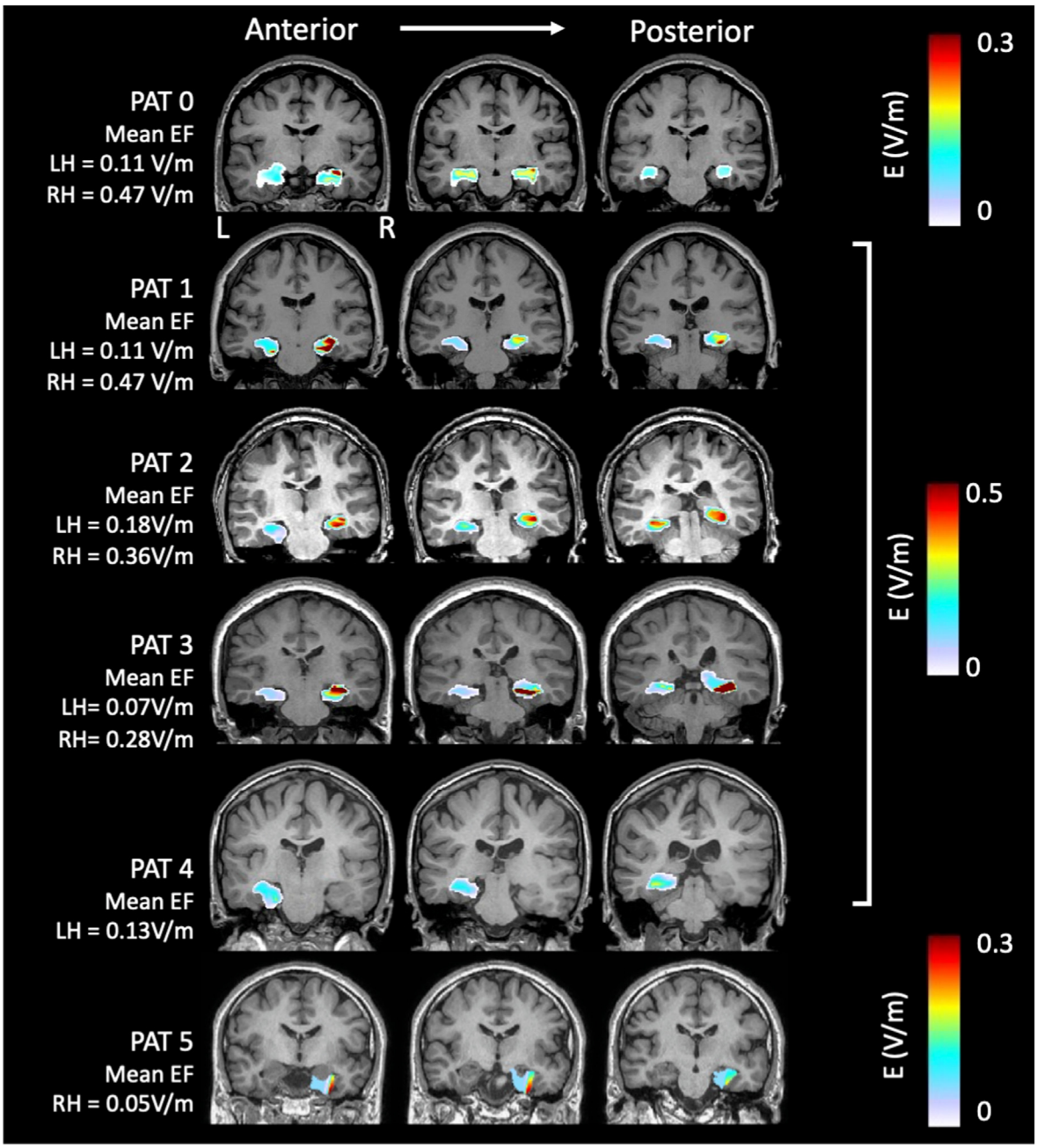

Fig. 4. Title: Spatial distribution of the electric field magnitudes in hippocampi using the full tensor calculation.
Caption: Coronal view of spatial distribution of the electric field magnitudes in hippocampi after calculating the full electric field (EF) tensor overlayed on individual patients' MRI. EF tensors were computed from the empirical values measured in SEEG contacts within the hippocampus. For each patient, three slices of interest are displayed (From left to right: anterior to posterior). (L: left, R: right, H: Hippocampus). (For interpretation of the references to color in this figure legend, the reader is referred to the Web version of this article.)

Table 1
Title : Means and standard deviations of the electric field magnitudes at 0.5 and 1 mA intensities in our cohort (EF: Electric field ; SEEG : stereoelectroencephalographic).

Patient	Nb of SEEG contacts	Mean EF at 0.5 mA ($V \cdot m^{-1}$)	Mean EF at 1 mA ($V \cdot m^{-1}$)
0	172	NA	0.16 (±0.19)
1	162	0.18 (±0.29)	0.36 (±0.58)
2	101	0.13 (±0.11)	0.24 (±0.22)
3	151	0.09 (±0.1)	0.17 (±0.20)
4	89	0.14 (±0.29)	0.26 (±0.58)
5	155	0.08 (±0.14)	0.16 (±0.29)
6	149	0.04 (±0.02)	0.08 (±0.04)
7	166	NA	0.13 (±0.27)

2.4.1. Deep brain structures investigation

We visually selected, thanks to the CT-MR co-registrations, SEEG contacts within the deep brain structures to study the EF in these regions. Electrophysiological data were checked by neurologists to confirm the previous selection and to determine boundaries between gray and white matter. Intracerebral SEEG contacts which recorded physiological brain activity were considered within the gray matter, and those which did not, were considered within the white matter [62]. Then, we calculated the mean and the standard deviation of the EF magnitudes in the deep brain structures (both right and left): amygdala, hippocampus, and cingulate gyrus. The mean was obtained by doing the same equation as (Eq. (5)) where n is the number of SEEG contacts within the deep structures and Ej the EF in the SEEG contact j (in the structures).

To estimate the EF in the entire volume of the deep brain structures, we calculated the EF tensors using the five following steps:

1. On the individual patient's MRI, anatomy was automatically labelled with CAT12 (a SPM12 toolbox) [63]. Thanks to this segmentation and labelling, different masks were generated: amygdala mask, hippocampus mask, cingulum mask (depending on the patient).
2. An interpolant F was calculated with the Matlab® function `F=scatteredInterpolant(x,y,z,v)` using all SEEG contacts (where x,y,z are the SEEG contact coordinates and v the measured voltage amplitudes) using a natural neighbor method [64].
3. The interpolated amplitudes were evaluated at the query points for each anatomical mask by calling F (qx,qy,qz) (where qx, qy and qz are the mask's voxel coordinates).
4. Then, the full gradient was calculated using the Matlab® function `gradient()`) on the evaluated interpolated amplitudes within each mask, which gave the electric field in the 3D space Ex, Ey, Ez.
5. The electric field magnitude was calculated in each voxel of the mask using $|E| = \sqrt{Ex^2 + Ey^2 + Ez^2}$. The mean and maximum interpolated EF were measured in each anatomical mask (hippocampus, amygdala, and in the cingulate gyrus).

Finally, a paired student's test was performed to compare the mean EF magnitudes and the mean tensor-based EF magnitudes in our population with the hypothesis H_0: the mean difference of mean EF magnitudes and mean tensor-based EF magnitudes is null.

2.5. Influence of tACS parameters

2.5.1. Influence of tACS frequency

To investigate the frequency dependence of the EF, we calculated the percentages of variation between the EF magnitudes obtained at different TES frequencies (1 Hz; 3 Hz; 7 Hz; 35 Hz; 71 Hz; 140 Hz) with the magnitudes obtained at the TES frequency of interest used in this study (i.e., 300 Hz). We calculated these variations as follows:

$$\%Variation(f) = \frac{1}{n}\sum_{i=1}^{n}\left(\frac{EF_i(f) - EF_i(f=300)}{EF_i(f=300)} \cdot 100\right)$$

With f the frequency tested, n the total number of intracerebral contacts.

This variation was calculated on all intracerebral contacts. Then, we calculated the difference (in $V \cdot m^{-1}$ and in percentage) of the mean EF magnitudes in the entire brain and the deep structures between the lowest (1 Hz) and the highest (300 Hz) frequencies.

2.5.2. Influence of tACS intensity

To investigate the impact of the tACS intensity, we calculated the EF values obtained at 0.5 mA and those obtained at 1 mA in all SEEG contacts. In order to discard SEEG contacts that could be saturated (especially at 1 mA), we used the `isoutlier()` Matlab function to remove the outliers which were over three standard deviations away from the mean of the error (i.e., the difference between measured and expected EF values).

A 1st degree polynomial linear regression was executed on the data ($E_1 = f(E_{0.5})$ with $E_{0.5}$ and E_1 the electric field distribution at 0.5 mA and at 1 mA, respectively) to estimate the coefficient of the given function. The fitted 1st degree polynomial curve can be expressed by:

$$E_1 = f(E_{0.5}) = p1 \cdot E_{0.5} + p2$$

where p1 (the slope) and p2 are the coefficients obtained from the model.

Then, we compared the empirical values E_1 with the predicted values E_{1th} (with a slope at exactly 2.00) by calculating the mean of the absolute difference (error) between E_1 and E_{1th} which can be considered as the Mean Absolute Error (MAE).

2.5.3. Influence of tACS montages

To investigate the impact of the tACS montage, a study was conducted with patient #7 (male 27 years old). Eighteen SEEG electrodes were implanted symmetrically in the same brain structures in both hemispheres (9 electrodes in each hemisphere) for a total of 203 intracerebral contacts (Fig. 1). SEEG electrodes sampled mainly the frontal lobe structures (cingulate gyri, supplementary motor areas, superior, middle, and inferior frontal gyri *e*tc.) and also both amygdalae. The principal objective was to investigate the impact of different tACS montages on the intracerebral EF values in deep brain structures.

Fifteen different montages based on the 10-10 system were used: C3-FT10; C3-T8; C3−C4; Cz-FT10; Cz-T8; Cz-C4; Fz-FT10; Fz-T8; Fz-C4; Fz-Cz; Fz-C3; Fz-T7, T7-FT10; T7-T8; T7-C4. Among these TES montages, we searched for those which gave the maximum mean EF value in the deep brain structures using empirical and tensor-based investigations (SEEG contacts in both hemispheres for amygdalae, anterior cingulate gyri, and middle cingulate gyri).

2.6. Influence of the depth

For every patient, the Euclidean distances between each intracerebral contact and the nearest TES electrode were measured. To study the influence of distance on EF magnitudes, we segmented the total distance in similarly sized segments and grouped EF magnitudes according to these segments. Then, we calculated the mean and median of the EF in each distance group. Next, assuming that the mean and median values would decrease as a function of the distance according to the inverse-square law, we performed a non-linear regression on those values by fitting a power curve expressed by:

$$f(d) = a \cdot \frac{1}{d^b} + c$$

where a, b and c are the non-linear regression coefficients and d the distance from the nearest TES electrode. Groups of EF magnitudes were displayed in violin plots by computing the density of the data distribution as a function of the depth.

3. Results

As expected, during TES, patients reported mild skin sensations (tickling) at both 0.5 mA and 1 mA intensities. No other side effects were noticed. No epileptic seizure was induced by the tACS experiments.

Altogether, patients had 1360 intracerebral SEEG contacts. The most superficial SEEG contacts, in addition to 21 SEEG contacts (which were detected as outliers) were discarded (n = 215). Therefore, this intracerebral EF study relied on 1145 SEEG contacts (average: 143 contacts/patient).

3.1. Intracerebral electric fields

Original data of this study, including individual anonymized MRI, SEEG electrode coordinates and EF magnitudes are available at Mendeley Data at: https://data.mendeley.com/datasets/sk279ktjv3/3.

Fig. 2A displays global EF distributions in our cohort (Patient #0–7).

In this population, 102 SEEG contacts sampled the deep brain structures: 42 were in the hippocampi, 28 in the amygdalae and 32 in the cingulate gyri (Table 2).

The mean and standard deviation (SD) of the EF in these deep brain structures were 0.14 ± 0.08 $V \cdot m^{-1}$.

The mean and SD of the EF in the hippocampi were 0.17 ± 0.06 $V \cdot m^{-1}$ with a maximum of 0.38 $V \cdot m^{-1}$ for a 1 mA stimulation (Fig. 3).

The mean and SD of the EF in the amygdala were 0.21 ± 0.08 $V \cdot m^{-1}$ with a maximum of 0.49 $V \cdot m^{-1}$ for a 1 mA stimulation.

The mean and SD of the EF in the cingulate gyri were 0.07 ± 0.02 $V \cdot m^{-1}$ with a maximum of 0.11 $V \cdot m^{-1}$ for a 1 mA stimulation.

The mean and SD of the tensor-based EF magnitudes were 0.16 ± 0.14 $V \cdot m^{-1}$, 0.19 ± 0.09 $V \cdot m^{-1}$ and 0.10 ± 0.07 $V \cdot m^{-1}$ for the hippocampi, amygdalae, and cingulate gyri, respectively (Fig. 4 for the spatial distribution in the hippocampus. For the full tensor, see supplementary data 2,3,4). There was no significant difference between the empirical mean EF values and the tensor-based mean EF values (paired student's *t*-test $p = 0.88$).

Table 2
Title : Electric field magnitudes in the deep brain structures.

Patient	Deep brain structures	Nb of SEEG contacts	Mean EF at 1 mA ($V \cdot m^{-1}$)	Mean tensor-based EF ($V \cdot m^{-1}$)	Max EF at 1 mA ($V \cdot m^{-1}$)	EF Value 1 ($V \cdot .m^{-1}$)	EF Value 2 ($V \cdot .m^{-1}$)	EF Value 3 ($V \cdot .m^{-1}$)	EF Value 4 ($V \cdot .m^{-1}$)	EF Value 5 ($V \cdot .m^{-1}$)
0	R Hippocampus	4	0.16	0.09	0.26	0.26	0.10	0.09	0.19	*NA*
	L Hippocampus	4	0.16	0.06	0.18	0.12	0.14	0.18	0.18	*NA*
	L Amygdala	4	0.22	0.09	0.25	0.25	0.24	0.21	0.20	*NA*
	L. Post Cingulate gyrus	2	0.06	*NA*	0.06	0.05	0.06	*NA*	*NA*	*NA*
1	R Hippocampus	4	0.24	0.47	0.29	0.21	0.23	0.24	0.29	*NA*
	L Hippocampus	4	0.21	0.11	0.23	0.19	0.19	0.21	0.23	*NA*
	L Amygdala	4	0.28	0.30	0.29	0.28	0.29	0.27	0.27	*NA*
2	L Hippocampus	5	0.19	0.07	0.22	0.20	0.19	0.18	0.17	0.22
	R Hippocampus	5	0.19	0.28	0.38	0.17	0.16	0.14	0.12	0.38
	L Amygdala	5	0.22	0.34	0.23	0.23	0.23	0.21	0.20	0.23
3	L Hippocampus	4	0.12	0.07	0.14	0.12	0.12	0.11	0.14	*NA*
	R Hippocampus	4	0.10	0.28	0.11	0.10	0.10	0.10	0.11	*NA*
	L Amygdala	4	0.14	0.10	0.14	0.14	0.14	0.14	0.13	*NA*
4	L Hippocampus	5	0.20	0.13	0.26	0.19	0.17	0.17	0.20	0.26
	L Amygdala	5	0.23	0.13	0.25	0.25	0.24	0.22	0.22	0.23
5	R Hippocampus	3	0.13	0.07	0.14	0.13	0.13	0.14	*NA*	*NA*
6	L. Ant Cingulate gyrus 1	2	0.09	0.08	0.1	0.08	0.10	*NA*	*NA*	*NA*
	L. Ant Cingulate gyrus 2	3	0.08		0.9	0.09	0.08	0.08	*NA*	*NA*
	L. mid Cingulate gyrus	2	0.06		0.06	0.05	0.06	*NA*	*NA*	*NA*
	R ant. Cingulate gyrus 1	2	0.10	0.08	0.1	0.09	0.10	*NA*	*NA*	*NA*
	R ant. Cingulate gyrus 2	2	0.09		0.09	0.08	0.09	*NA*	*NA*	*NA*
	R. mid Cingulate gyrus	2	0.07		0.06	0.06	0.07	*NA*	*NA*	*NA*
7	L ant. Cingulate gyrus	3	0.06	0.18	0.07	0.07	0.06	0.06	*NA*	*NA*
	L mid. Cingulate gyrus 1	3	0.07		0.08	0.07	0.07	0.08	*NA*	*NA*
	L mid. Cingulate gyrus 2	2	0.06		0.07	*NA*	0.05	0.07	*NA*	*NA*
	R ant. Cingulate gyrus	3	0.05	0.14	0.07	0.04	0.05	0.07	*NA*	*NA*
	R mid. Cingulate gyrus 1	3	0.07		0.07	0.07	0.06	0.07	*NA*	*NA*
	R mid. Cingulate gyrus 2	3	0.09		0.11	0.11	0.09	0.07	*NA*	*NA*
	L Amygdala	3	0.13	0.20	0.13	0.13	0.13	0.12	*NA*	*NA*
	R Amygdala	3	0.24	0.18	0.49	0.11	0.11	0.49	*NA*	*NA*

3.2. Influence of tACS parameters

3.2.1. Influence of tACS frequency

Fig. 2B and supplementary data 4 display global EF distributions of patient #0 according to tACS frequencies. In the entire brain and in the deep brain structures, compared to EF magnitudes at 300 Hz, global EF magnitudes varied around of 9 ± 8% and 5 ± 7%. Overall, the mean EF magnitudes at 1 Hz were 15% lower than at 300 Hz (i.e., −0.02 $V \cdot m^{-1}$). In opposition, in the deep brain structures, the mean EF magnitudes at 1Hz were 11% higher than at 300Hz (i.e., +0.03 $V \cdot m^{-1}$).

3.2.2. Influence of tACS intensity

6 patients were included for the EF magnitude comparison between a 0.5 mA and a 1 mA stimulation (2 datasets of 807 values; Patients #1–6). The measured slope (p1) from the linear regression varied from 2 (Patient #1–5) to 2.2 (Patient #6), and the determination coefficients ranged from $R^2 = 0.98$ (Patient #6) to $R^2 = 1.00$ (Patients #3–5) (see supplementary data 1 Fig. 6). Finally, the comparison of the empirical values to the predicted ones (with a slope exactly at 2.00) showed a MAE from 0.0003 (Patient #6) to 0.0174 (Patient #1). These values demonstrated EF is doubled when stimulation intensity is doubled.

3.2.3. Influence of tACS montage

Fig. 2C displays global EF distributions of patient #7 according to tACS montages. 166 SEEG contacts in patient #7 were used to analyze the influence of the TES montages. Fourteen montages were included in the analysis, and one was discarded (Fz-T7: noisy data). Seventeen contacts were in the cingulate gyri and 6 contacts in the amygdalae. There was no contact in the hippocampus.

In these deep brain structures, the TES montage which yielded the highest mean EF in the amygdalae was T7-T8 (0.24 $V \cdot m^{-1}$) and in the cingulate gyri was T7-C4 (0.09 $V \cdot m^{-1}$) (Table 3). The TES montage, which yielded the lowest mean EF was Fz-Cz for the deep brain structures investigated.

The highest tensor-based mean EF estimations showed the same effective montage (T7-T8) for the amygdalae (0.41 $V \cdot m^{-1}$) and Fz-C4 for the cingulate gyri (0.42 $V \cdot m^{-1}$) (supplementary data 3). Fz-Cz montage was also the montage which yielded the lowest mean EF.

3.3. Influence of the depth

The maximum distance from the nearest TES electrode and a SEEG contact was 14.6 cm. Ten segments of 1.5 cm were defined from 0 cm to 15 cm and EF magnitudes were grouped according to these segments. No EF magnitudes were found between 0 cm and 1.5 cm.

The measured coefficients from the non-linear regression on the median (black dashed line in Fig. 2D) EF distribution across groups were: $a = 1.28$ (0.92, 1.63), $b = -1.76$ (with −2.13 and −1.39 as the 95% confidence bounds), $c = 0.03$ (0.01, 0.05) and a determination coefficient of $R^2 = 0.99$.

The measured coefficients from the non-linear regression on the mean (red dashed line in Fig. 2D) EF distribution across groups were: $a = 2.8$ (2.1, 3.51); $b = -1.65$ (−1.99, −1.31); $c = 0.03$ (−0.02, 0.07) and a determination coefficient of $R^2 = 0.99$.

Fig. 2E displays global distribution of the EF magnitudes in the entire brain and the deep brain structures in our cohort.

4. Discussion

The human *in-vivo* estimation of electric field during TES poses great technical and methodological challenges. While the simultaneous combination of intracerebral human EEG recordings with TES could greatly contribute to this endeavor, it is rare - only a few clinical contexts require intracerebral recordings in humans such as Parkinson's disease or drug-resistant epilepsies [41,46–48] - and also highly challenging. To the best of our knowledge, compared to previous *in-vivo* human studies, our study included a higher number of patients and is the first to measure the intracerebral EF with a high number of SEEG contacts generated by low intensity-tACS using small HD electrodes.

SEEG is particularly relevant for the intracerebral EF investigation. First, it offers a high spatial resolution in depth, which makes the EF investigation from superficial to deep brain structures possible. Second, it relies on the implantation of depth electrodes through very small guide screws inserted into the skull, which do not require craniotomy where a bone flap is temporally removed from the skull to access the brain. Computational studies have shown that skull defects from craniotomies impact brain sources stimulations [49] or localizations [65,66]. For instance, in the TES context, Datta et al. demonstrated that a craniotomy (moderate/large skull defect) leads to an increase of peak cortical EF, especially when one stimulating electrode was placed over the skull defects [49]. In our study, the size of the skull defect (2.45 mm-diameter) is at least 30 times smaller than the size of a craniotomy (around 7-10 cm-diameter) performed during epilepsy surgery. In addition, craniotomy induces breach rhythms, which cause an increase in the amplitude of alpha, beta, and mu rhythms, leading to the breach effect [54]. In tACS studies at low frequencies in patients with craniotomy (e.g., electrocorticography investigation), the high voltage of breach rhythms can induce artifacts on the signal and so mis-estimation of the EF. In contrast, in the present study, thanks to simultaneous EEG-SEEG recording performed before the tACS investigation, there was no breach rhythm detected. Further, compared to Opitz et al. [46], who placed TES electrodes (25 cm^2) over both temples close to SEEG electrodes' holes (right and left temporal lobes), our study placed small TES electrodes far (at least 5 cm) from the first holes performed for the SEEG investigation. Thus, the impact of the "craniotomy" performed during the SEEG implantation in our study should be low, if not negligible, in the EF measurement. It is also worth mentioning that, according to

Table 3
Title : Electric field magnitudes according to differents tACS montages in patient #7.

Mean EF magnitudes ($V \cdot m^{-1}$)	Cz-FT10	Cz-T8	Cz-C4	C3-FT10	C3-T8	C3–C4	T7-FT10	T7-T8	T7-C4	Fz-FT10	Fz-T8	Fz-C4	Fz-Cz	Fz-C3
L ant. cingulate gyrus	0.03	0.03	0.06	0.06	0.05	0.04	0.06	0.05	0.05	0.05	0.04	0.05	0.01	0.01
L mid. cingulate gyrus 1	0.04	0.04	0.07	0.07	0.07	0.04	0.06	0.06	0.05	0.05	0.05	0.05	0.02	0.01
L mid. cingulate gyrus 2	0.03	0.03	0.06	0.06	0.06	0.02	0.04	0.05	0.05	0.04	0.05	0.04	0.02	0.00
R ant. cingulate gyrus	0.01	0.02	0.04	0.03	0.04	0.01	0.04	0.05	0.05	0.01	0.02	0.01	0.00	0.02
R mid. cingulate gyrus 1	0.02	0.03	0.06	0.05	0.06	0.01	0.05	0.06	0.07	0.01	0.02	0.01	0.01	0.04
R mid. cingulate gyrus 2	0.00	0.02	0.05	0.04	0.08	0.02	0.05	0.06	0.09	0.02	0.00	0.02	0.00	0.05
L Amygdala	0.05	0.04	0.10	0.11	0.09	0.06	0.13	0.12	0.11	0.06	0.05	0.06	0.00	0.05
R Amygdala	0.11	0.09	0.18	0.12	0.17	0.05	0.17	0.24	0.22	0.05	0.11	0.05	0.00	0.08

simultaneous EEG-SEEG studies of brain source detections, the volume conduction can be considered as being normal (i.e., without currents leakage and breach rhythms) [67–69].

Two previous studies investigated the global intracerebral EF using only SEEG recordings ([46], n = 1 patient; [41], n = 1 patient) and two studies investigated the intracerebral EF in the subthalamic nuclei and internal globus pallidus ([47], n = 3 patients; [48], n = 1). However, the methodology and objectives of these four studies (regarding both recording and stimulating) differed substantially from ours. First, our study used SEEG recording coupled with low intensity tACS, small electrodes, and no craniotomy. Second, we showed the ability of TES to reach the deep limbic structures (cingulate gyrus, hippocampus, and amygdala) with a mean electric field of 0.14 $V \cdot m^{-1}$ at 1 mA intensity. Despite the relatively low numbers of SEEG contacts, which were not homogeneously located (on a 3D grid) in the deep structures due to clinical constraints, the tensors-based EF magnitude confirmed our results. Thus, pending further validation of our results in a larger cohort, our study suggests that low-intensity TES can be proposed for neuromodulation of deep brain structures.

Interestingly, our findings showed values higher than those required to induce neural entrainment and stochastic effects (at lower frequency TES) [11,14,18,19,70]. Our results bring fundamental biophysical evidence supporting the promising results of deep structure neuromodulation using TES [31,32,71,72]. In a previous paper, we demonstrated that the volume conduction laws applied from deep electrical brain sources (epileptic focus) to scalp electrodes [68]. Therefore, we expected that the volume conduction laws applied from a scalp electrical source (TES electrodes) to the deep brain structures.

Our current study provides empirical evidence that the reciprocity principle used in few TES studies [73,74] can also apply to deep brain sources. From a biophysical point of view, we also showed that the EF magnitudes in the entire brain, according to the depth, followed the same distribution as Huang et al. [41]. As expected, because of the biophysical properties, EF magnitudes decreased as a function of the depth following a power-curve with coefficients close to the inverse-square law value (theoretically $b = 2$). The presence of low EF magnitudes in the most external parts of the brain can be explained by the positions between the current sources (i.e., the stimulating scalp electrodes) and the SEEG contacts.

In the present study, we found a strong correlation between the intracerebral electric field magnitude and the TES intensity at 300 Hz. As expected, when the stimulation intensity doubles, the electric field strength doubles as well. Huang et al. qualitatively reported this linearity on the intracerebral voltage measurements [41]. Assuming the purely resistive nature of the head tissues (quasi-static assumption), which was confirmed by our results on the tACS frequency investigation, this linear relationship between stimulation intensity and EF magnitudes can be extrapolated for other TES frequency stimulations. In addition, we did not observe body resistance reduction, contrary to Chhatbar et al. who used tDCS and demonstrated this phenomenon when stimulation intensity increased [47]. One plausible account of this discrepancy could be that the alternative current of tACS does not polarize the tissues as tDCS does. Therefore, the body resistance would be less affected by tACS. Considering both the recent tDCS studies which used 4 mA [47,75–77] and our own observations (i.e., a mean of 0.14 $V \cdot m^{-1}$ EF in the deep brain structures and the linear relationship between intensity and EF magnitudes), we would expect higher electric fields.

Computational studies have demonstrated the importance of the target's orientation regarding the current flow [78,79], the stimulation electrodes' position [26,57,80,81], and a detailed head tissues modeling [27,82–85]. The two studies which compared, predicted and measured EF in humans reported good correlations ($0.70 \leq r \leq 0.75$) but not perfect predictions ($0.50 \leq r^2 \leq 0.58$) [41,85]. The extrapolation of these studies needs further investigation and validation using human *in-vivo* datasets. In our study, we showed that the TES montages producing the strongest EF in deep brain structures were those with the longest distance between the TES electrodes (i.e., minimal scalp shunt). The smaller EF magnitudes in the cingulate gyri (by comparison to the complex amygdala/hippocampus) can be explained by the orientation of the SEEG electrodes. Also, the low empirical EF magnitudes found with TES montages of the closest electrodes (such as Fz-Cz) seem to reflect the scalp shunt phenomenon. These results are in line with a recent computational study [57].

Despite its original contribution and strengths, our study also has limitations. First, due to the rare and challenging combination of TES and SEEG recordings, the study still includes a relatively low number of patients (especially for the influence of TES montages). Our findings should therefore encourage additional research in the field of intracerebral EF estimation in human *in-vivo* for both methodological and fundamental (neuromodulation) purposes. The second limitation is that the influence of TES frequency was evaluated in one subject only, while the tACS parameters were limited to 300 Hz and 1 min stimulation in all other individual brains tested. However, the choice of 300 Hz was particularly adapted to this methodological study of intracerebral EF investigation because it falls in a frequency band where electrophysiological activity of the human brain is low. In the entire brain, we observed an increase (15%) of the mean EF magnitudes in function of the frequency. This finding is in opposition to the one from Opitz *et al.* This difference could be explained by some discrepancies. First, the anatomical and biophysical properties between species (humans versus monkeys) differ. Second, the number and the positions of the intracerebral contacts in the brain volume differ: 172 contacts with a perpendicular implantation (left to right) in our study versus 64 contacts with a tangential implantation (posterior to anterior) in Opitz *et al.* Third, we calculated the raw electric fields at the difference to Opitz *et al.*, who calculated the mean normalized voltages. Contrary to our finding in the entire brain, our experiment (Patient #0) exhibited mean EF magnitudes in deep brain structures at 1 Hz 11% higher than at 300 Hz. So, our EF magnitudes in the deep brain structures at 300 Hz are representative of the fields generated by low frequency tACS [86,87] or tDCS studies [7].

Finally, the influence of TES montage was also evaluated in one patient only. Thus, our data showing different EF magnitudes according to TES montages need to be confirmed and extended with additional individual brain tested. In doing so, this investigation would help validate computational studies and establish guidelines for bipolar TES electrodes placement.

CRediT authorship contribution statement

Samuel Louviot: Methodology, Software, Investigation, Formal analysis, Writing – original draft. **Louise Tyvaert:** Resources, Writing – review & editing, Clinical, Validation. **Louis G. Maillard:** Resources, Writing – review & editing, Clinical, Validation. **Sophie Colnat-Coulbois:** Resources, Writing – review & editing, Clinical, Validation. **Jacek Dmochowski:** Conceptualization, Methodology, Software, Resources, Formal analysis, Writing – review & editing, Funding acquisition. **Laurent Koessler:** Conceptualization, Methodology, Resources, Validation, Writing – review & editing, Funding acquisition, Supervision.

Declaration of competing interest

We wish to draw the attention of the Editor to the following facts which may be considered as potential conflicts of interest: Jacek Dmochowski has patent rights to HD-tDCS technology.

We confirm that the manuscript has been read and approved by all named authors and that there are no other persons who satisfied the criteria for authorship but are not listed. We further confirm that the order of authors listed in the manuscript has been approved by all of us.

Acknowledgements

This study was funded by grants from the Lorraine University of Excellence Initiative (France) and the City College of New-York (USA) (DrEAM mobility grant) and the Rotary Club of Nancy (France). The authors thank Mr. Pierre Riff for the data acquisition and Bruno Rossion for his comments.

Appendix A. Supplementary data

Supplementary data to this article can be found online at https://doi.org/10.1016/j.brs.2021.11.001.

References

[1] Stagg CJ, Nitsche MA. Physiological basis of transcranial direct current stimulation. Neuroscientist 2011;17:37–53. https://doi.org/10.1177/1073858410386614.
[2] Reato D, Rahman A, Bikson M, Parra LC. Effects of weak transcranial alternating current stimulation on brain activity—a review of known mechanisms from animal studies. Front Hum Neurosci 2013;7:1–8. https://doi.org/10.3389/fnhum.2013.00687.
[3] Filmer HL, Dux PE, Mattingley JB. Applications of transcranial direct current stimulation for understanding brain function. Trends Neurosci 2014;37:742–53. https://doi.org/10.1016/j.tins.2014.08.003.
[4] Boggio PS, Ferrucci R, Rigonatti SP, Covre P, Nitsche M, Pascual-Leone A, et al. Effects of transcranial direct current stimulation on working memory in patients with Parkinson's disease. J Neurol Sci 2006;249:31–8. https://doi.org/10.1016/j.jns.2006.05.062.
[5] Schlaug G, Renga V, Nair D. Transcranial direct current stimulation in stroke recovery. Arch Neurol 2008;65:1571–6. https://doi.org/10.1001/archneur.65.12.1571.
[6] Tortella G. Transcranial direct current stimulation in psychiatric disorders. World J Psychiatr 2015;5:88. https://doi.org/10.5498/wjp.v5.i1.88.
[7] Lefaucheur JP. A comprehensive database of published tDCS clinical trials (2005–2016). Neurophysiol Clin 2016;46:319–98. https://doi.org/10.1016/j.neucli.2016.10.002.
[8] Jackson MP, Rahman A, Lafon B, Kronberg G, Ling D, Parra LC, et al. Animal models of transcranial direct current stimulation: methods and mechanisms. Clin Neurophysiol 2016;127:3425–54. https://doi.org/10.1016/j.clinph.2016.08.016.
[9] Bikson M, Inoue M, Akiyama H, Deans JK, Fox JE, Miyakawa H, et al. Effect of uniform extracellular DC electric fields on excitability in rat hippocampal slices in vitro. J Physiol 2004;557:175–90. https://doi.org/10.1113/jphysiol.2003.055772.
[10] Jefferys JG. Influence of electric fields on the excitability of granule cells in Guinea-pig hippocampal slices. J Physiol 1981;319:143–52. https://doi.org/10.1113/jphysiol.1981.sp013897.
[11] Francis JT, Gluckman BJ, Schiff SJ. Sensitivity of neurons to weak electric fields. J Neurosci 2003;23:7255–61. https://doi.org/10.1523/JNEUROSCI.23-19-07255.2003.
[12] Rahman A, Reato D, Arlotti M, Gasca F, Datta A, Parra LC, et al. Cellular effects of acute direct current stimulation: somatic and synaptic terminal effects. J Physiol 2013;591:2563–78. https://doi.org/10.1113/jphysiol.2012.247171.
[13] Reato D, Bikson M, Parra LC. Lasting modulation of in vitro oscillatory activity with weak direct current stimulation. J Neurophysiol 2015;113:1334–41. https://doi.org/10.1152/jn.00208.2014.
[14] Reato D, Rahman A, Bikson M, Parra LC. Low-intensity electrical stimulation affects network dynamics by modulating population rate and spike timing. J Neurosci 2010;30:15067–79. https://doi.org/10.1523/JNEUROSCI.2059-10.2010.
[15] Gluckman BJ, Neel EJ, Netoff TI, Ditto WL, Spano ML, Schiff SJ. Electric field suppression of epileptiform activity in hippocampal slices. J Neurophysiol 1996;76:4202–5. https://doi.org/10.1152/jn.1996.76.6.4202.
[16] Parra LC, Bikson M. Model of the effect of extracellular fields on spike time coherence. In: Annu. Int. Conf. IEEE Eng. Med. Biol. - Proc., vol. 26 VI, Conf Proc IEEE Eng med Biol Soc; 2004. p. 4584–7. https://doi.org/10.1109/iembs.2004.1404271.
[17] Terzuolo CA, Bullock TH. Measurement of imposed voltage gradient adequate to modulate neuronal firing. Proc Natl Acad Sci Unit States Am 1956;42:687–94. https://doi.org/10.1073/pnas.42.9.687.
[18] Deans JK, Powell AD, Jefferys JGR. Sensitivity of coherent oscillations in rat hippocampus to AC electric fields. J Physiol 2007;583:555–65. https://doi.org/10.1113/jphysiol.2007.137711.
[19] Liu A, Vöröslakos M, Kronberg G, Henin S, Krause MR, Huang Y, et al. Immediate neurophysiological effects of transcranial electrical stimulation. Nat Commun 2018;9. https://doi.org/10.1038/s41467-018-07233-7.
[20] Miranda PC, Lomarev M, Hallett M. Modeling the current distribution during transcranial direct current stimulation. Clin Neurophysiol 2006;117:1623–9. https://doi.org/10.1016/j.clinph.2006.04.009.
[21] Wagner T, Fregni F, Fecteau S, Grodzinsky A, Zahn M, Pascual-Leone A. Transcranial direct current stimulation: a computer-based human model study. Neuroimage 2007;35:1113–24. https://doi.org/10.1016/j.neuroimage.2007.01.027.
[22] Datta A, Bansal V, Diaz J, Patel J, Reato D, Bikson M. Gyri-precise head model of transcranial direct current stimulation: improved spatial focality using a ring electrode versus conventional rectangular pad. Brain Stimul 2009;2. https://doi.org/10.1016/j.brs.2009.03.005.
[23] Ruffini G, Wendling F, Merlet I, Molaee-Ardekani B, Mekonnen A, Salvador R, et al. Transcranial current brain stimulation (tCS): models and technologies. IEEE Trans Neural Syst Rehabil Eng 2013;21:333–45. https://doi.org/10.1109/TNSRE.2012.2200046.
[24] Saturnino GB, Antunes A, Thielscher A. On the importance of electrode parameters for shaping electric field patterns generated by tDCS. Neuroimage 2015;120:25–35. https://doi.org/10.1016/j.neuroimage.2015.06.067.
[25] Ramaraju S, Roula MA, McCarthy PW. Modelling the effect of electrode displacement on transcranial direct current stimulation (tDCS). J Neural Eng 2018;15. https://doi.org/10.1088/1741-2552/aa8d8a.
[26] Opitz A, Yeagle E, Thielscher A, Schroeder C, Mehta AD, Milham MP. On the importance of precise electrode placement for targeted transcranial electric stimulation. Neuroimage 2018;181:560–7. https://doi.org/10.1016/j.neuroimage.2018.07.027.
[27] Huang Y, Parra LC. Can transcranial electric stimulation with multiple electrodes reach deep targets? Brain Stimul 2019;12:30–40. https://doi.org/10.1016/j.brs.2018.09.010.
[28] Bikson M, Dmochowski J. What it means to go deep with non-invasive brain stimulation. Clin Neurophysiol 2020;131:752–4. https://doi.org/10.1016/j.clinph.2019.12.003.
[29] Krause MR, Vieira PG, Csorba BA, Pilly PK, Pack CC. Transcranial alternating current stimulation entrains single-neuron activity in the primate brain. Proc Natl Acad Sci U S A 2019;116:5747–55. https://doi.org/10.1073/pnas.1815958116.
[30] Vieira PG, Krause MR, Pack CC. tACS entrains neural activity while somatosensory input is blocked. PLoS Biol 2020;18. https://doi.org/10.1371/journal.pbio.3000834.
[31] Tekturk P, Erdogan ET, Kurt A, Vanli-yavuz EN, Ekizoglu E, Kocagoncu E, et al. The effect of transcranial direct current stimulation on seizure frequency of patients with mesial temporal lobe epilepsy with hippocampal sclerosis. Clin Neurol Neurosurg 2016;149:27–32. https://doi.org/10.1016/j.clineuro.2016.07.014.
[32] San-Juan D, Espinoza López DA, Vázquez Gregorio R, Trenado C, Fernández-González Aragón M, Morales-Quezada L, et al. Transcranial direct current stimulation in mesial temporal lobe epilepsy and hippocampal sclerosis. Brain Stimul 2017;10:28–35. https://doi.org/10.1016/j.brs.2016.08.013.
[33] Assenza G, Campana C, Assenza F, Pellegrino G, Di Pino G, Fabrizio E, et al. Cathodal transcranial direct current stimulation reduces seizure frequency in adults with drug-resistant temporal lobe epilepsy: a sham controlled study. Brain Stimul 2017;10:333–5. https://doi.org/10.1016/j.brs.2016.12.005.
[34] Khatoun A, Asamoah B, Laughlin MM. How does transcranial alternating current stimulation entrain single-neuron activity in the primate brain? Proc Natl Acad Sci U S A 2019;116:22438–9. https://doi.org/10.1073/pnas.1912927116.
[35] Asamoah B, Khatoun A, Mc Laughlin M. tACS motor system effects can be caused by transcutaneous stimulation of peripheral nerves. Nat Commun 2019;10:266. https://doi.org/10.1038/s41467-018-08183-w.
[36] Adair D, Truong D, Esmaeilpour Z, Gebodh N, Borges H, Ho L, et al. Electrical stimulation of cranial nerves in cognition and disease. Brain Stimul 2020;13:717–50. https://doi.org/10.1016/j.brs.2020.02.019.
[37] Vanneste S, Mohan A, Yoo H Bin, Huang Y, Luckey AM, Lauren McLeod S, et al. The peripheral effect of direct current stimulation on brain circuits involving memory. Sci Adv 2020;6:1–19. https://doi.org/10.1126/SCIADV.AAX9538.
[38] Underwood E. Cadaver study challenges brain stimulation methods: unusual test of transcranial stimulation shows that little electrical current penetrates the skull. Science 2016;352(80):397. https://doi.org/10.1126/science.352.6284.397.
[39] Vöröslakos M, Takeuchi Y, Brinyiczki K, Zombori T, Oliva A, Fernández-Ruiz A, et al. Direct effects of transcranial electric stimulation on brain circuits in rats and humans. Nat Commun 2018;9. https://doi.org/10.1038/s41467-018-02928-3.
[40] Lafon B, Henin S, Huang Y, Friedman D, Melloni L, Thesen T, et al. Low frequency transcranial electrical stimulation does not entrain sleep rhythms

measured by human intracranial recordings. Nat Commun 2017;8:1199. https://doi.org/10.1038/s41467-017-01045-x.
[41] Huang Y, Liu AA, Lafon B, Friedman D, Dayan M, Wang X, et al. Measurements and models of electric fields in the in vivo human brain during transcranial electric stimulation. Elife 2017;6:1–27. https://doi.org/10.7554/eLife.18834.
[42] Akhtari M, Bryant HC, Mamelak AN, Flynn ER, Heller L, Shih JJ, et al. Conductivities of three-layer line human skull. Brain Topogr 2002;14:151–67. https://doi.org/10.1023/A:1014590923185.
[43] Dasilva AF, Mendonca ME, Zaghi S, Lopes M, Dossantos MF, Spierings EL, et al. TDCS-induced analgesia and electrical fields in pain-related neural networks in chronic migraine. Headache 2012;52:1283–95. https://doi.org/10.1111/j.1526-4610.2012.02141.x.
[44] DaSilva AF, Truong DQ, DosSantos MF, Toback RL, Datta A, Bikson M. State-of-art neuroanatomical target analysis of high-definition and conventional tDCS montages used for migraine and pain control. Front Neuroanat 2015;9:89. https://doi.org/10.3389/fnana.2015.00089.
[45] Gomez-Tames J, Asai A, Hirata A. Significant group-level hotspots found in deep brain regions during transcranial direct current stimulation (tDCS): a computational analysis of electric fields. Clin Neurophysiol 2020;131:755–65. https://doi.org/10.1016/j.clinph.2019.11.018.
[46] Opitz A, Falchier A, Yan CG, Yeagle EM, Linn GS, Megevand P, et al. Spatiotemporal structure of intracranial electric fields induced by transcranial electric stimulation in humans and nonhuman primates. Sci Rep 2016;6:1–11. https://doi.org/10.1038/srep31236.
[47] Chhatbar PY, Kautz SA, Takacs I, Rowland NC, Revuelta GJ, George MS, et al. Evidence of transcranial direct current stimulation-generated electric fields at subthalamic level in human brain in vivo. Brain Stimul 2018;11:727–33. https://doi.org/10.1016/j.brs.2018.03.006.
[48] Ruhnau P, Rufener KS, Heinze HJ, Zaehle T. Sailing in a sea of disbelief: in vivo measurements of transcranial electric stimulation in human subcortical structures. Brain Stimul 2018;11:241–3. https://doi.org/10.1016/j.brs.2017.09.015.
[49] Datta A, Bikson M, Fregni F. Transcranial direct current stimulation in patients with skull defects and skull plates: high-resolution computational FEM study of factors altering cortical current flow. Neuroimage 2010;52:1268–78. https://doi.org/10.1016/j.neuroimage.2010.04.252.
[50] Isnard J, Taussig D, Bartolomei F, Bourdillon P, Catenoix H, Chassoux F, et al. French guidelines on stereoelectroencephalography (SEEG). Neurophysiol Clin 2018;48:5–13. https://doi.org/10.1016/j.neucli.2017.11.005.
[51] Salado AL, Koessler L, DeMijolla G, Schmitt E, Vignal JP, Civit T, et al. sEEG is a safe procedure for a comprehensive anatomic exploration of the insula: a retrospective study of 108 procedures representing 254 transopercular insular electrodes. Oper Neurosurg 2018;14:1–8. https://doi.org/10.1093/ons/opx106.
[52] Almukhtar A, Ju X, Khambay B, McDonald J, Ayoub A. Comparison of the accuracy of voxel based registration and surface based registration for 3D assessment of surgical change following orthognathic surgery. PLoS One 2014;9:1–6. https://doi.org/10.1371/journal.pone.0093402.
[53] Jacques C, Jonas J, Maillard L, Colnat-Coulbois S, Rossion B, Koessler L. Fast periodic visual stimulation to highlight the relationship between human intracerebral recordings and scalp electroencephalography. Hum Brain Mapp 2020;41:2373–88. https://doi.org/10.1002/hbm.24952.
[54] Brigo F, Cicero R, Fiaschi A, Bongiovanni LG. The breach rhythm. Clin Neurophysiol 2011;122:2116–20. https://doi.org/10.1016/j.clinph.2011.07.024.
[55] Tadel F, Baillet S, Mosher JC, Pantazis D, Leahy RM. Brainstorm: a user-friendly application for MEG/EEG analysis. Comput Intell Neurosci 2011;2011:13. https://doi.org/10.1155/2011/879716.
[56] Koessler L, Maillard L, Benhadid A, Vignal JP, Felblinger J, Vespignani H, et al. Automated cortical projection of EEG sensors: anatomical correlation via the international 10-10 system. Neuroimage 2009;46:64–72. https://doi.org/10.1016/j.neuroimage.2009.02.006.
[57] Faria P, Hallett M, Miranda PC. A finite element analysis of the effect of electrode area and inter-electrode distance on the spatial distribution of the current density in tDCS. J Neural Eng 2011;8. https://doi.org/10.1088/1741-2560/8/6/066017.
[58] Datta A, Elwassif M, Battaglia F, Bikson M. Transcranial current stimulation focality using disc and ring electrode configurations: FEM analysis. J Neural Eng 2008;5:163–74. https://doi.org/10.1088/1741-2560/5/2/007.
[59] Frigo M, Johnson SG. The design and implementation of FFTW3. Proc IEEE 2005;93:216–31. https://doi.org/10.1109/JPROC.2004.840301.
[60] Hofmanis J, Caspary O, Louis-Dorr V, Maillard L. Automatic depth electrode localization in intracranial space. In: 4th Int. Conf. Bio-inspired Syst. Signal process. Biosignals 2011. Rome, Italy: CDROM; 2011.
[61] Ashburner J, Friston KJ. Unified segmentation. Neuroimage 2005;26:839–51. https://doi.org/10.1016/j.neuroimage.2005.02.018.
[62] Koessler L, Colnat-Coulbois S, Cecchin T, Hofmanis J, Dmochowski JP, Norcia AM, et al. In-vivo measurements of human brain tissue conductivity using focal electrical current injection through intracerebral multicontact electrodes. Hum Brain Mapp 2017;38:974–86. https://doi.org/10.1002/hbm.23431.
[63] Rolls ET, Huang CC, Lin CP, Feng J, Joliot M. Automated anatomical labelling atlas 3. Neuroimage 2020:206. https://doi.org/10.1016/j.neuroimage.2019.116189.
[64] Amidror I. Scattered data interpolation methods for electronic imaging systems: a survey. J Electron Imag 2002;11:157. https://doi.org/10.1117/1.1455013.
[65] Benar CG, Gotman J. Modeling of post-surgical brain and skull defects in the EEG inverse problem with boundary element models. Neuroimage 2000;11. https://doi.org/10.1016/s1053-8119(00)91564-7.
[66] Lau S, Güllmar D, Flemming L, Grayden DB, Cook MJ, Wolters CH, et al. Skull defects in finite element head models for source reconstruction from magnetoencephalography signals. Front Neurosci 2016;10:141. https://doi.org/10.3389/fnins.2016.00141.
[67] Jacques C, Jonas J, Maillard L, Colnat-Coulbois S, Rossion B, Koessler L. Fast periodic visual stimulation to highlight the relationship between human intracerebral recordings and scalp electroencephalography. Hum Brain Mapp 2020:1–16. https://doi.org/10.1002/hbm.24952.
[68] Koessler L, Cecchin T, Colnat-Coulbois S, Vignal JP, Jonas J, Vespignani H, et al. Catching the invisible: mesial temporal source contribution to simultaneous EEG and SEEG recordings. Brain Topogr 2014;28:5–20. https://doi.org/10.1007/s10548-014-0417-z.
[69] Gavaret M, Dubarry AS, Carron R, Bartolomei F, Trébuchon A, Bénar CG. Simultaneous SEEG-MEG-EEG recordings Overcome the SEEG limited spatial sampling. Epilepsy Res 2016;128:68–72. https://doi.org/10.1016/j.eplepsyres.2016.10.013.
[70] Kato I, Innami K, Sakuma K, Miyakawa H, Inoue M, Aonishi T. Frequency-dependent entrainment of spontaneous Ca transients in the dendritic tufts of CA1 pyramidal cells in rat hippocampal slice preparations by weak AC electric field. Brain Res Bull 2019;153:202–13. https://doi.org/10.1016/j.brainresbull.2019.08.009.
[71] Khan A, Wang X, Ti CHE, Tse CY, Tong KY. Anodal transcranial direct current stimulation of anterior cingulate cortex modulates subcortical brain regions resulting in cognitive enhancement. Front Hum Neurosci 2020;14:584136. https://doi.org/10.3389/fnhum.2020.584136.
[72] Verveer I, Hill AT, Franken IHA, Yücel M, van Dongen JDM, Segrave R. Modulation of Control: can HD-tDCS targeting the dACC reduce impulsivity? Brain Res 2021:1756. https://doi.org/10.1016/j.brainres.2021.147282.
[73] Fernández-Corazza M, Turovets S, Luu P, Anderson E, Tucker D. Transcranial electrical neuromodulation based on the reciprocity principle. Front Psychiatr 2016;7:1–19. https://doi.org/10.3389/fpsyt.2016.00087.
[74] Dmochowski JP, Koessler L, Norcia AM, Bikson M, Parra LC. Optimal use of EEG recordings to target active brain areas with transcranial electrical stimulation. Neuroimage 2017;157:69–80. https://doi.org/10.1016/j.neuroimage.2017.05.059.
[75] Nitsche MA, Bikson M. Extending the parameter range for tDCS: safety and tolerability of 4 mA stimulation. Brain Stimul 2017;10:541–2. https://doi.org/10.1016/j.brs.2017.03.002.
[76] Chhatbar PY, Chen R, Deardorff R, Dellenbach B, Kautz SA, George MS, et al. Safety and tolerability of transcranial direct current stimulation to stroke patients – A phase I current escalation study. Brain Stimul 2017;10:553–9. https://doi.org/10.1016/j.brs.2017.02.007.
[77] Khadka N, Borges H, Paneri B, Kaufman T, Nassis E, Zannou AL, et al. Adaptive current tDCS up to 4 mA. Brain Stimul 2020;13:69–79. https://doi.org/10.1016/j.brs.2019.07.027.
[78] Dmochowski JP, Datta A, Bikson M, Su Y, Parra LC. Optimized multi-electrode stimulation increases focality and intensity at target. J Neural Eng 2011;8. https://doi.org/10.1088/1741-2560/8/4/046011.
[79] Rawji V, Ciocca M, Zacharia A, Soares D, Truong D, Bikson M, et al. tDCS changes in motor excitability are specific to orientation of current flow. Brain Stimul 2018;11:289–98. https://doi.org/10.1016/j.brs.2017.11.001.
[80] Faria P, Leal A, Miranda PC. Comparing different electrode configurations using the 10-10 international system in tDCS: a finite element model analysis. In: Proc. 31st Annu. Int. Conf. IEEE Eng. Med. Biol. Soc. Eng. Futur. Biomed. EMBC 2009, vol. 2009. IEEE Computer Society; 2009. p. 1596–9. https://doi.org/10.1109/IEMBS.2009.5334121.
[81] Gomez-Tames J, Asai A, Mikkonen M, Laakso I, Tanaka S, Uehara S, et al. Group-level and functional-region analysis of electric-field shape during cerebellar transcranial direct current stimulation with different electrode montages. J Neural Eng 2019;16. https://doi.org/10.1088/1741-2552/ab0ac5.
[82] Laakso I, Tanaka S, Koyama S, De Santis V, Hirata A. Inter-subject variability in electric fields of motor cortical tDCS. Brain Stimul 2015;8:906–13. https://doi.org/10.1016/j.brs.2015.05.002.
[83] Lee C, Jung YJ, Lee SJ, Im CH. COMETS2: an advanced MATLAB toolbox for the numerical analysis of electric fields generated by transcranial direct current stimulation. J Neurosci Methods 2017;277:56–62. https://doi.org/10.1016/j.jneumeth.2016.12.008.
[84] Saturnino GB, Madsen KH, Thielscher A. Electric field simulations for transcranial brain stimulation using FEM: an efficient implementation and error analysis. J Neural Eng 2019;16. https://doi.org/10.1088/1741-2552/ab41ba.
[85] Puonti O, Saturnino GB, Madsen KH, Thielscher A. Value and limitations of intracranial recordings for validating electric field modeling for transcranial brain stimulation. Neuroimage 2020;208:116431. https://doi.org/10.1016/j.neuroimage.2019.116431.
[86] Elyamany O, Leicht G, Herrmann CS, Mulert C. Transcranial alternating current stimulation (tACS): from basic mechanisms towards first applications in psychiatry. Eur Arch Psychiatr Clin Neurosci 2021;271:135–56. https://doi.org/10.1007/s00406-020-01209-9.
[87] Antal A, Paulus W. Transcranial alternating current stimulation (tACS). Front Hum Neurosci 2013;7:1–4. https://doi.org/10.3389/fnhum.2013.00317.